

Supporting information for “Surface inducing high-temperature superconductivity in layered metal carbides Li_2BC_3 and LiBC by metallizing σ electrons”

Muyao Wang¹, Xiaohan Liu¹, Xiaowei Huang^{1†}, Liangliang Liu^{1,2,3*}

¹Key Laboratory for Special Functional Materials of Ministry of Education, School of Materials Science and Engineering, Henan University, Kaifeng, 475004, China

²Institute of Quantum Materials and Physics, Henan Academy of Sciences, Zhengzhou, 450046, China

³Joint Center for Theoretical Physics, Henan University, Kaifeng 475004, China

1. The electronic structures and electron-phonon coupling of bulk Li_2BC_3 .

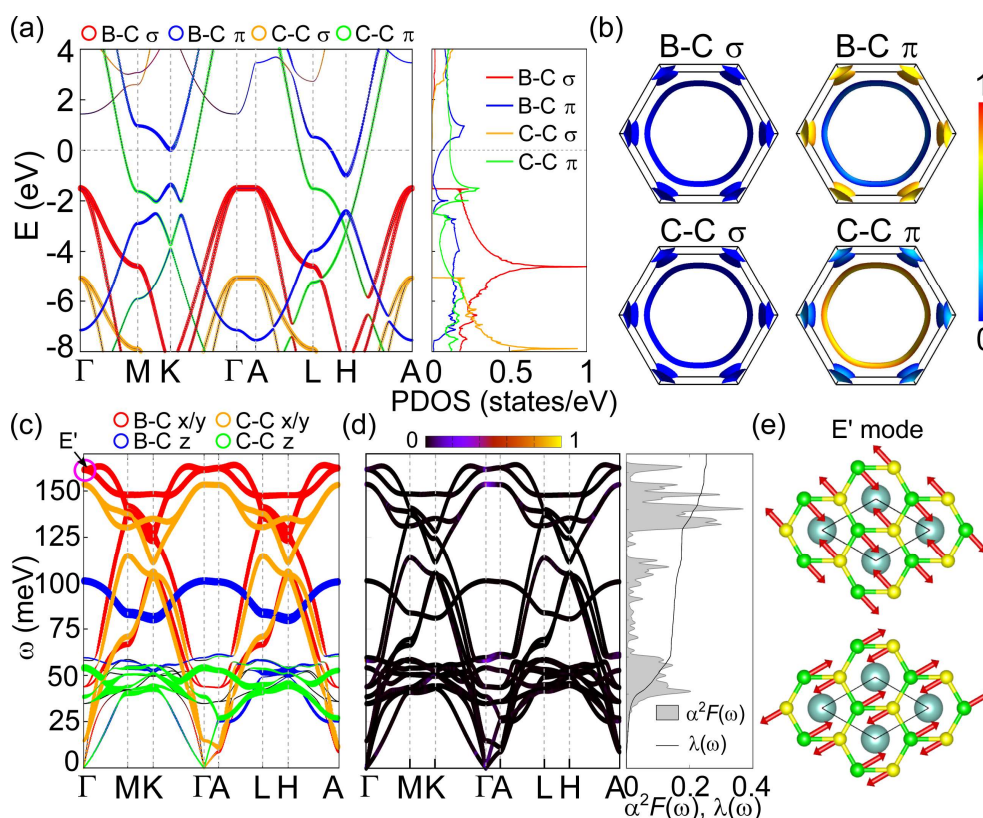


Figure S1: (a) Calculated band structure and partial density of states (PDOS), together with projection of their electronic states onto the σ -bonding states of B-C/C-C p_x/p_y orbitals and the π -bonding states of B-C/C-C p_z orbitals, respectively. (b) The corresponding Fermi sheets. The electronic states on the Fermi surface (FS) are projected onto B-C/C-C σ orbitals and B-C/C-C π orbitals, respectively. (c) The calculated phonon spectrums with projection of the in-plane and out-of-plane vibration modes of the B-C/C-C layers. (d) Phonon spectrum with projection of EPC strength λ_{qv} using the color scale in the range [0, 1]. (e) The vibration patterns E' of two B-C in-plane stretching modes, as marked in (c).

Here, we note that because B-C/C-C σ states are far away from the E_F and the dominant B-C/C-C π states have weak coupling with B-C/C-C out-of-plane vibrations,

the obtained total λ is only 0.23. Accordingly, the estimated T_c is smaller than 1 K for the bulk Li_2BC_3 .

2. All configurations of Li_2BC_3 and LiBC (0001) surfaces and corresponding surface energies

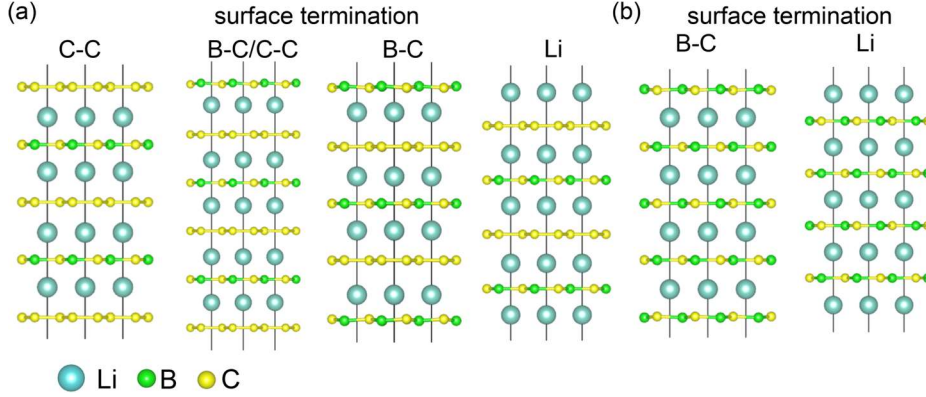


Figure S2: The possible configurations with different terminations for (a) Li_2BC_3 and (b) LiBC (0001) surfaces.

Surface termination	E_{surf} (eV/Å ²)	Surface termination	E_{surf} (eV/Å ²)
(Li_2BC_3) C-C	0.051	(LiBC) Li	0.165
(Li_2BC_3) B-C/C-C	0.078	(LiBC) B-C	0.195
(Li_2BC_3) B-C	0.106	(LiBC) B-B	0.097
(Li_2BC_3) Li	0.117	(LiBC) Al	0.060

Table S1: The calculated surface energies (E_{surf}) of different Li_2BC_3 and LiBC (0001) surface configurations. The calculated equation is below: $E_{surf} = \frac{E_{slab} - E_{bulk}}{2 \times S}$, in which E_{slab} and E_{bulk} are the total energies of the surface slab and bulk configurations, respectively. S is the surface area of the slab configuration, and the number 2 represents the upper and down surfaces of the slab configurations.

For the (0001) surfaces of Li_2BC_3 and LiBC , there could be different atomic layers as the terminated surface. Figures S2(a)-(b) show all kinds of configurations of Li_2BC_3 and LiBC (0001) surfaces, and the corresponding surface energies are listed in Table S1. It is noted that Li_2BC_3 (0001) surface with symmetrical C-C termination [see Figure S2 (a)] has the lowest energies of 0.051 eV/Å², while this surface cannot have the high- T_c superconductivity because near Fermi level, the dominant components are B-C/C-C π states, which has weak electron-phonon coupling, similar to the case of bulk Li_2BC_3 [see Figure S1]. For our predicted Li_2BC_3 (0001) surfaces with symmetrical B-C termination or unsymmetrical B-C and C-C terminations [see Figure S2(a)], which could host high- T_c surface superconductivity, the results show they all have slightly higher surface energies of 0.106 eV/Å² and 0.078 eV/Å² [see Table S1]. For another

LiBC (0001) surface, there are two possible surface configurations with symmetrical B-C termination or Li termination [see Figure S2(b)]. The calculated surface energy displays that LiBC (0001) surface with symmetrical Li termination has a lower energy of 0.165 eV/\AA^2 , and B-C terminated surface has a disadvantage in energy, about 0.03 eV/\AA^2 .

Therefore, for our predicted high- T_c surface systems, that is, Li_2BC_3 (0001) surfaces with symmetrical B-C termination or unsymmetrical B-C and C-C terminations and LiBC (0001) surface with B-C termination, we hope that the targeted experiments are able to synthesize these high-quality surface samples and further verify our predictions of high-temperature superconductivity by the advanced experimental technology, considering AlB_2 (0001) surface with the B-B termination have been synthesized in previous researches [1] although it has a higher surface energy based on our calculations [see Table S1].

3. The structure, band structure, density of states of Li_2BC_3 with unsymmetrical B-C and C-C terminations.

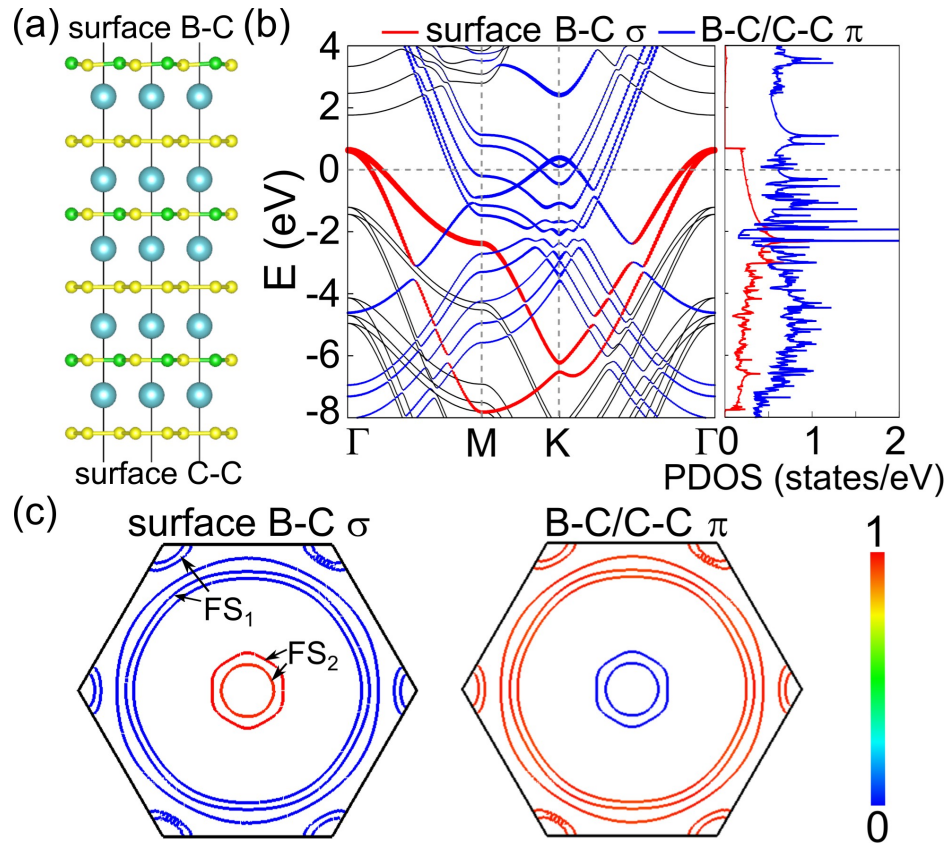


Figure S3: (a) The optimized configuration of Li_2BC_3 (0001) surface with unsymmetrical B-C and C-C terminations. (b) Calculated band structure and partial density of states (PDOS), together with projection of their electronic states onto projected onto the surface B-C σ orbitals and all B-C π orbitals, respectively. (c) The corresponding Fermi sheets. The electronic states on the Fermi surface are projected onto surface B-C σ orbitals and all B-C π orbitals, respectively.

4. The superconducting properties of Li_2BC_3 with unsymmetrical B-C and C-C terminations.

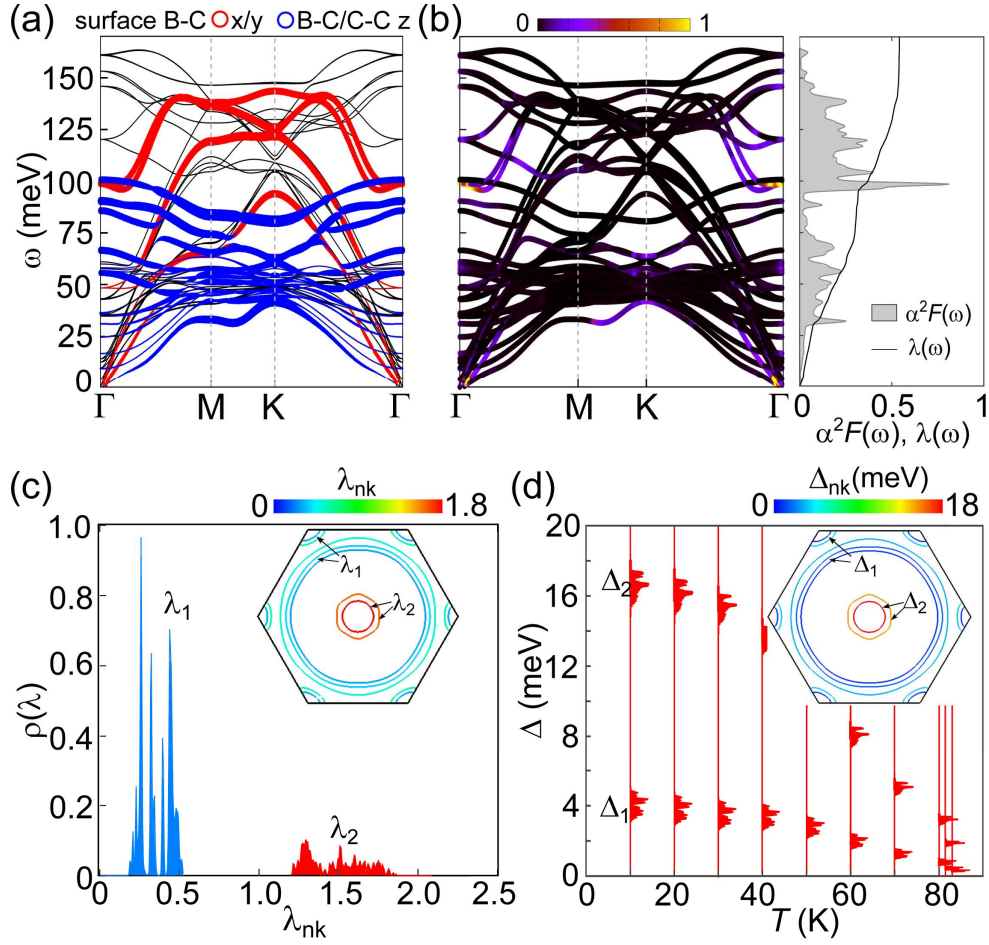


Figure S4: (a) Phonon spectrums with the projection of surface B-C in-plane vibrations and all B-C/C-C out-of-plane vibrations. (b) Phonon spectrum with projection of EPC strength $\lambda_{\text{q}\nu}$ using the color scale in the range $[0, 1]$, and the isotropic Eliashberg spectral function $\alpha^2F(\omega)$ with the integrated isotropic EPC constant $\lambda(\omega)$. (c) Distribution $\rho(\lambda)$ of k -resolved EPC constant λ_{nk} associated with the projection of the λ_{nk} onto each FS sheet. The two separated regimes of λ_{nk} are indicated as λ_1 and λ_2 . (d) Energy distribution of the anisotropic superconducting gap Δ of Li_2BC_3 surface as a function of temperature T . The two separated gaps are indicated as Δ_1 and Δ_2 . The inset is k -resolved superconducting gaps Δ_{nk} on the Fermi surface at 10 K. Here, the obtained T_c is ~ 83 K.

5. The structures, band structures and density of states of Li_2BC_3 surface modes with different layer thicknesses.

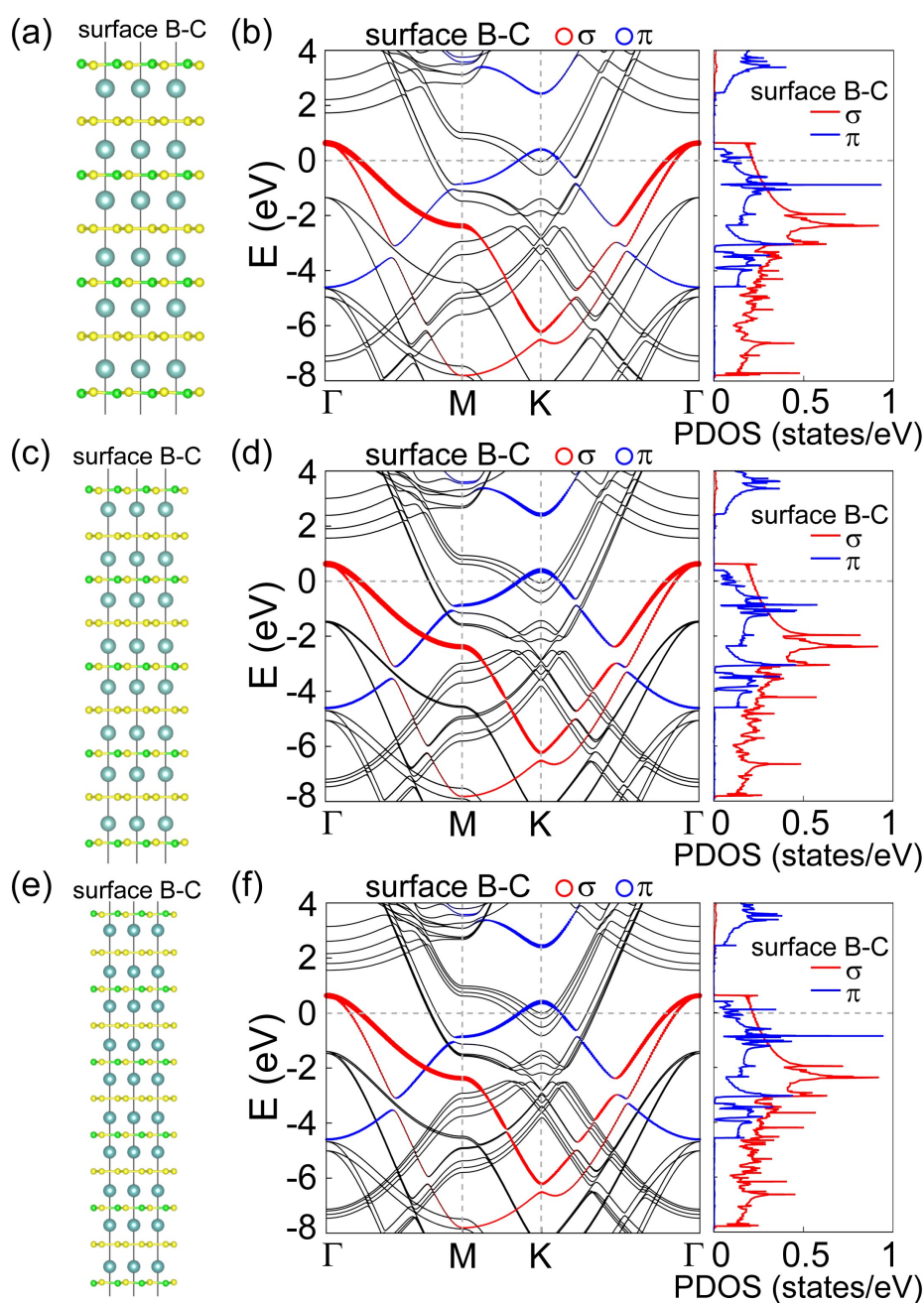


Figure S5: (a) Li_2BC_3 surface model consists of six Li layers and seven B-C/C-C layers, and (b) shows the corresponding band structure and PDOS with projected onto surface B-C σ and π orbitals. (c) Li_2BC_3 surface models consists of eight Li layers and nine B-C/C-C layers, and (d) shows the corresponding band structure and PDOS with projected onto surface B-C σ and π orbitals. (e) Li_2BC_3 surface models consists of ten Li layers and eleven B-C/C-C layers, and (f) shows the corresponding band structure and PDOS with projected onto surface B-C σ and π orbitals.

6. The band structure and density of states of bulk LiBC.

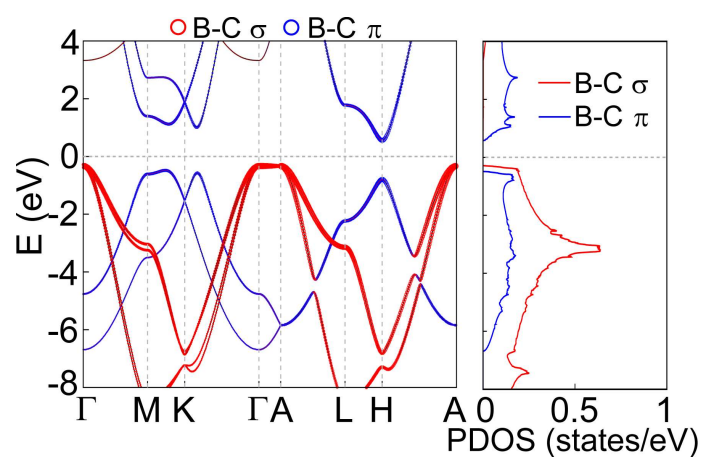


Figure S6: Calculated band structure and partial density of states (PDOS), together with projection of their electronic states onto the σ -bonding states of B-C p_x/p_y orbitals and the π -bonding states of B-C p_z orbitals, respectively.

7. The structures, band structures and density of states of LiBC surface models with different layer thicknesses.

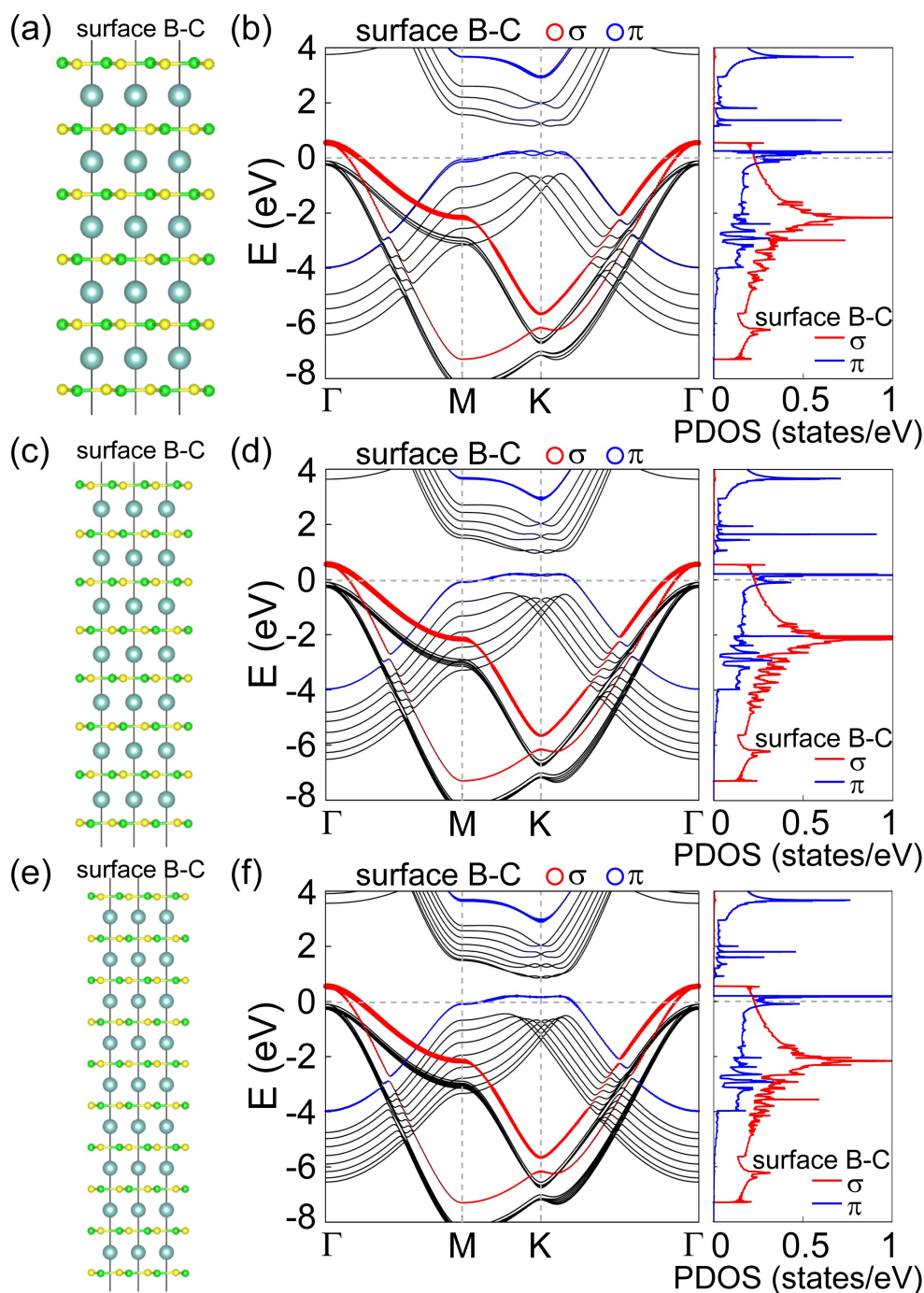


Figure S7: (a) LiBC surface model consists of five Li layers and six B-C layers, and (b) shows the corresponding band structure and PDOS with projected onto surface B-C σ and π orbitals. (c) LiBC surface models consists of seven Li layers and eight B-C layers, and (d) shows the corresponding band structure and PDOS with projected onto surface B-C σ and π orbitals. (e) LiBC surface model consists of nine Li layers and ten B-C layers, and (f) shows the corresponding band structure and PDOS with projected onto surface B-C σ and π orbitals.

8. The vibration modes of bulk LiBC layers

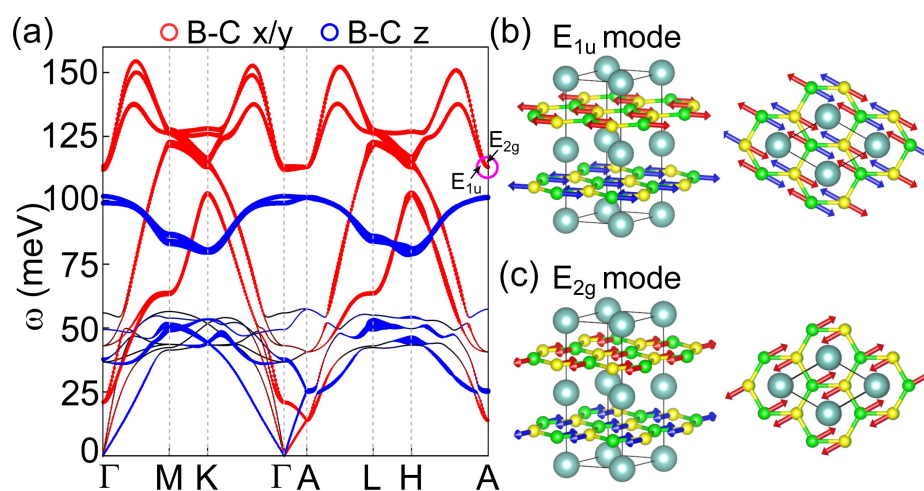


Figure S8: (a) The calculated phonon spectrum of bulk LiBC with the weighted atom-vibration modes. (b) and (c) show the in-plane stretching modes (E_{1u} and E_{2g}) of B-C layers.

9. The vibration patterns of surface B-C in-plane modes

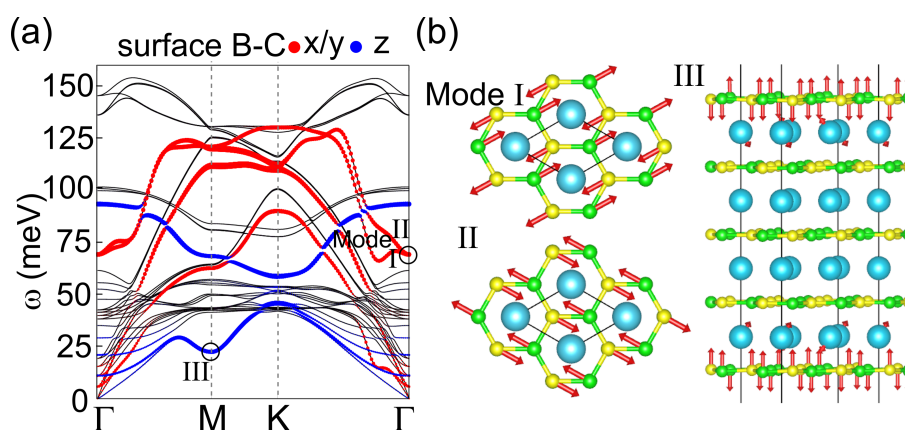


Figure S9: (a) The calculated phonon spectrum of LiBC surface with the projection of surface B-C in-plane vibration modes. (b) The vibration patterns of surface B-C in-plane stretching Modes I and II, and vibration pattern of out-of-plane Mode III.

10. The calculated electron-phonon coupling of LiBC surface

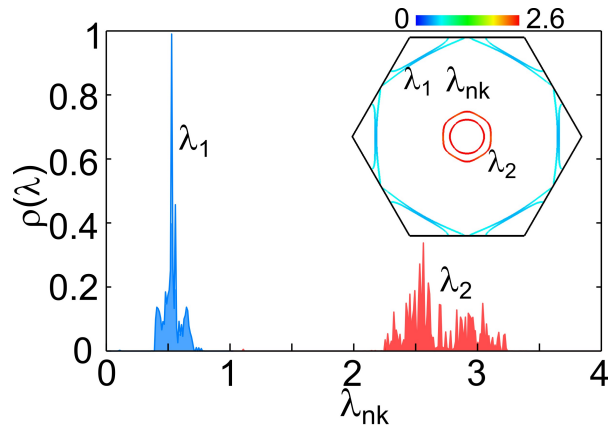


Figure S10: Distribution $\rho(\lambda)$ of k -resolved EPC constant λ_{nk} and the projection of the λ_{nk} on each FS sheet. The two separated regimes of λ_{nk} are indicated as λ_1 and λ_2 .

11. The calculated electronic structures of MgB₂ film

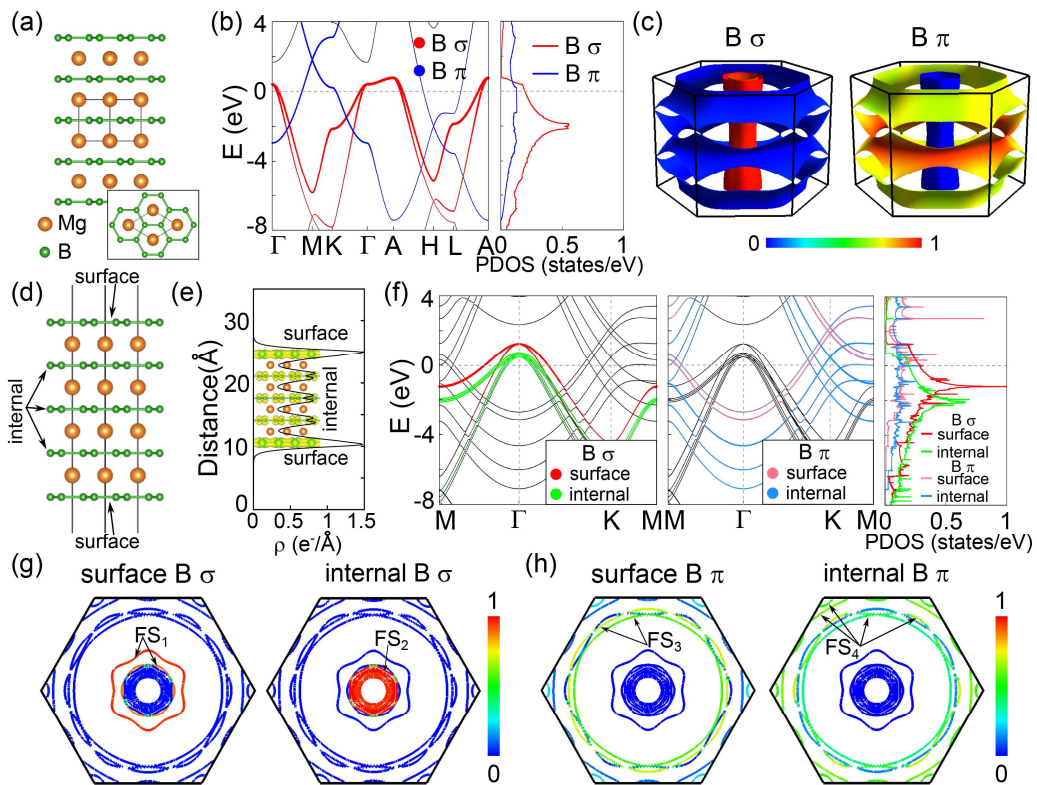


Figure S11: (a) The structure of bulk MgB₂. (b) Calculated band structure and partial density of states (PDOS) for bulk MgB₂, together with (c) distribution of B σ (p_x/p_y) and π (p_z) orbitals on the Fermi surface using the color scale in the range [0,1]. (d) The optimized MgB₂ surface with B termination. (e) Calculated partial charge density of MgB₂ surface. (f) Band structure of MgB₂ surface together with PDOS, as projected onto the surface B σ/π orbitals, and internal B σ/π orbitals. (g) Distribution of surface

and internal B σ orbitals and (h) surface and internal π orbitals on the Fermi surface using the color scale in the range [0,1].

The previous experimental and theoretical researches have studied the superconductivity of MgB₂ film, and reported that surface would suppress the electron-phonon coupling (EPC) and SC with the T_c reduced to ~ 30 K from the 39 K of bulk [2-5], while the detailed microscopic mechanism is still absent. Here, we redo the superconducting calculation to clearly exhibit the role of surface in superconductivity (SC) of MgB₂ film.

Figs. S11(a)-(c) shows the calculated band structure, density of states (DOS) and Fermi surface (FS) of bulk MgB₂. It is seen that different from the cases of bulks LiBC and Li₂BC₃, in which B-C σ states are below the Fermi level (E_F) [see Fig. S1 and Fig. S5 of Supporting information], the B σ states in bulk MgB₂ are crossing the E_F and exhibit the metallic property. The reason is that the attractive potential of Mg²⁺ between B layers lowers the π bands of B layers, resulting in σ - π charge transfer that drives the hole doping of the σ bands [6]. Accordingly, the metallic σ states of B layer could effectively couple with the B in-plane stretching modes, giving rise to the large EPC constant and high T_c of 39 K in bulk MgB₂ [6,7].

To study the superconducting properties of MgB₂ (0001) surface, the symmetrical surface slab model with B termination is adopted, as shown in Fig. S11(d). It is seen that in this structure, there are two kind of B layers, i.e., one is the surface exposed layer, and the other are internal layers, which have similar coordination environments to B layer of bulk MgB₂. Here, in MgB₂ surface, considering that there are two kinds of B layers (surface and internal) and orbitals (σ and π), the calculated band structure and PDOS are projected on the surface and internal B σ/π orbitals, respectively (see Fig. S11(f)). Naturally, the FS sheets can be divided into four independent parts according to the orbital distributions, as shown in Figs. S11(g) and S11(h), and these sheets are marked as the FS₁, FS₂, FS₃ and FS₄, respectively. It is seen that because surface symmetry reduction induces hole self-doping into surface B layer, its σ -bonding states are driving to move upward energetically associated with the new emergency of a larger hexagon FS sheet (i.e., the FS₁). Accordingly, surface B layer obtains a larger electronic occupation near E_F , and its σ -bonding strength gets enhanced compared to those of internal B layers [see the calculated DOS in Fig. S11(f) and partial charge distribution in Fig. S11(e)]. These calculated results are consistent with the previous report that surface could enhance σ states and its bonding nature of surface B layer in MgB₂ film [2,5].

12. The superconducting properties of MgB₂ film

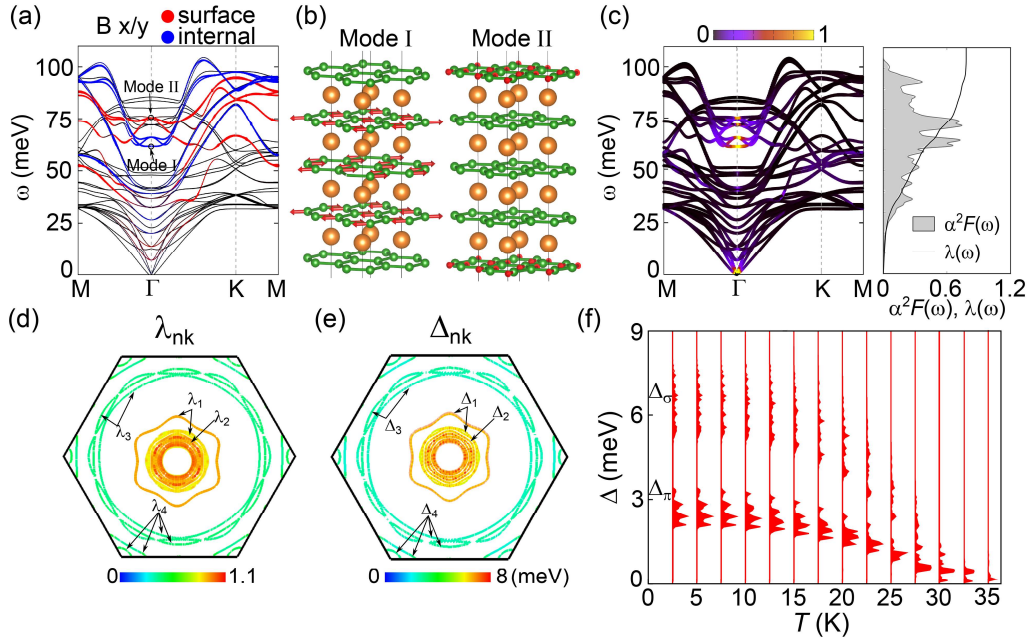


Figure S12: (a) The phonon spectrum with the projection of surface and bulk B in-plane vibration modes. (b) Atomic displacements of the Modes I for internal B layers and Mode II for the surface B layers, labeled as indicated in (a). (c) Phonon spectrum with projection of EPC strength λ_{qv} using the color scale in the range [0,1], and the isotropic Eliashberg spectral function $\alpha^2 F(\omega)$ with the integrated isotropic EPC constant $\lambda(\omega)$. (d) Projection of the k -resolved EPC constant λ_{nk} on each FS sheet. (e) Projection of k -resolved superconducting gaps Δ_{nk} on each FS sheet. (f) Energy distribution of the anisotropic superconducting gap Δ of MgB₂ surface as a function of temperature T .

Here, we turn to examine the vibration properties and EPC of MgB₂ surface. Fig. S11(a) shows the calculated phonon spectrum with the projection of surface and internal B in-plane vibrations. Here, it is worth noting that compared to the internal B vibrations [such as Mode I in Fig. S12 (b)], surface B in-plane stretching mode at Γ point (such as Mode II in Fig. S12) gets stiffness due to the enhanced σ -bonding strength, and their phonon energies are increased to ~ 75 meV from ~ 62 meV of internal B layers (B layer in bulk MgB₂: ~ 62.6 meV). This feature is totally different from the case of LiBC and Li₂BC₃ surfaces that surface induces phonon softness. Accordingly, the calculated EPC strength λ_{qv} in Fig. S12(c) shows that these stiffed surface phonon modes result in the decrease of the values λ_{qv} to ~ 0.8 , while the values λ_{qv} contributed by internal B layers are ~ 1.0 . Additionally, this surface-weakened EPC strength is also manifested by the k -resolved EPC constant λ_{nk} , as shown in Fig. S12(d). It is seen that the FS₁ contributed by surface B-C σ states, has a relatively small value of $\lambda_1 = \sim 0.8$, compared to the $\lambda_2 = \sim 1.0$ of the FS₂ contributed by the internal B σ states [see Fig. S11(g) and Fig. S12(d)]. Naturally, surface B σ states produce a smaller superconducting gap. Fig. S11(e) shows that the value Δ_1 contributed by the FS₁ is ~ 7 meV, while the value Δ_2 by the FS₂ is ~ 8 meV. The Δ_1 and Δ_2 together form the superconducting gap Δ_σ [see Fig. S12(f)], and the Δ_3 and Δ_4 contributed by the FS₃ and FS₄ of surface and internal B π states together form the superconducting gap Δ_π . With the temperature T increasing, the gap Δ_σ combined with gap Δ_π produced get closed around 35 K, indicating the T_c is 35 K in

MgB₂ surface, which is slightly smaller than $T_c = 39$ K of bulk. This calculation is consistent with previous experimental and theoretical results [3,4], and gives a clear explanation that surface phonon stiffness suppresses the SC in MgB₂ film.

Reference

- [1] V. Sunko, D. Milosavljević, F. Mazzola, O. J. Clark, U. Burkhardt, T. K. Kim, H. Rosner, Yu. Grin, A. P. Mackenzie, and P. D. C. King, Surface and bulk electronic structure of aluminium diboride, *Phys. Rev. B*, 102, 035143 (2020).
- [2] I. G. Kim, J. I. Lee, B. I. Min, and A. J. Freeman, Surface electronic structures of superconducting thin film MgB₂(0001). *Phys. Rev. B*, 64, 020508 (2001).
- [3] J. Bekaert, L. Bignardi, A. Aperis, P. van Abswoude, C. Mattevi, S. Gorovikov, L. Petaccia, A. Goldoni, B. Partoens, P. M. Oppeneer, F. M. Peeters, M. V. Milosevic, P. Rudolf, and C. Cepek, Free surfaces recast superconductivity in few-monolayer MgB₂: Combined first-principles and ARPES demonstration. *Scientific Reports*, 7, 14458 (2017).
- [4] H. Schmidt, J. F. Zasadzinski, K. E. Gray, and D. G. Hinks, Energy gap from tunneling and metallic contacts onto MgB₂: Possible evidence for a weakened surface layer. *Phys. Rev. B*, 63, 220504 (2001).
- [5] Z. Y. Li, J. L. Yang, J. G. Hou, and Q. S. Zhu, First-principles study of MgB₂ (0001) surfaces. *Phys. Rev. B*, 65, 100507 (2002).
- [6] J. M. An and W. E. Pickett, Superconductivity of MgB₂: Covalent bonds driven metallic. *Phys. Rev. Lett.*, 86, 4366 (2001).
- [7] H. J. Choi, D. Roundy, H. Sun, M. L. Cohen, and S. G. Louie, The origin of the anomalous superconducting properties of MgB₂. *Nature (London)* 418, 758 (2002).